Time course analysis of sensory axon regeneration *in vivo* by directly tracing regenerating axons

Yan Gao[1, #], Yi-Wen Hu[2, #], Run-Shan Duan[3], Shu-Guang Yang[4], Feng-Quan Zhou[4, *], Rui-Ying Wang[2, *]

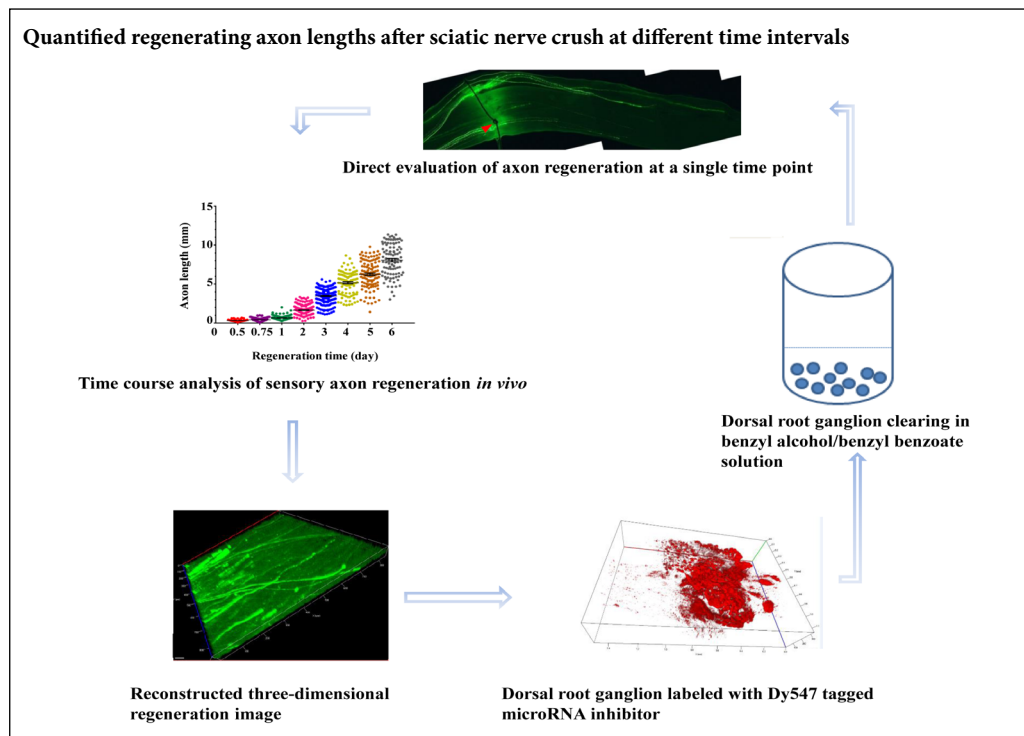1 Guilin Medical University, Guilin, Guangxi Zhuang Autonomous Region, China
2 Department of Orthopedic Surgery, Affiliated Hospital of Guilin Medical University, Guilin, Guangxi Zhuang Autonomous Region, China
3 Department of Orthopedics, Henan Provincial People's Hospital, People's Hospital of Zhengzhou University, Zhengzhou, Henan Province, China
4 Department of Orthopedic Surgery, Johns Hopkins University School of Medicine, Baltimore, MD, USA

Graphical Abstract

Quantified regenerating axon lengths after sciatic nerve crush at different time intervals

Direct evaluation of axon regeneration at a single time point

Time course analysis of sensory axon regeneration *in vivo*

Reconstructed three-dimensional regeneration image

Dorsal root ganglion labeled with Dy547 tagged microRNA inhibitor

Dorsal root ganglion clearing in benzyl alcohol/benzyl benzoate solution

Abstract

Most current studies quantify axon regeneration by immunostaining regeneration-associated proteins, representing indirect measurement of axon lengths from both sensory neurons in the dorsal root ganglia and motor neurons in the spinal cord. Our recently developed method of *in vivo* electroporation of plasmid DNA encoding for enhanced green fluorescent protein into adult sensory neurons in the dorsal root ganglia provides a way to directly and specifically measure regenerating sensory axon lengths in whole-mount nerves. A mouse model of sciatic nerve compression was established by squeezing the sciatic nerve with tweezers. Plasmid DNA carrying enhanced green fluorescent protein was transfected by ipsilateral dorsal root ganglion electroporation 2 or 3 days before injury. Fluorescence distribution of dorsal root or sciatic nerve was observed by confocal microscopy. At 12 and 18 hours, and 1, 2, 3, 4, 5, and 6 days of injury, lengths of regenerated axons after sciatic nerve compression were measured using green fluorescence images. Apoptosis-related protein caspase-3 expression in dorsal root ganglia was determined by western blot assay. We found that *in vivo* electroporation did not affect caspase-3 expression in dorsal root ganglia. Dorsal root ganglia and sciatic nerves were successfully removed and subjected to a rapid tissue clearing technique. Neuronal soma in dorsal root ganglia expressing enhanced green fluorescent protein or fluorescent dye-labeled microRNAs were imaged after tissue clearing. The results facilitate direct time course analysis of peripheral nerve axon regeneration. This study was approved by the Institutional Animal Care and Use Committee of Guilin Medical University, China (approval No. GLMC201503010) on March 7, 2014.

Key Words: axon regeneration; cell apoptosis; dorsal root ganglion; in vivo electroporation; microRNAs; peripheral nervous system; sciatic nerve; tissue clearing

Introduction

Axon regeneration is crucial for recovery of function after nervous system injury. The adult mammalian central nervous system (CNS) cannot be functionally recovered after injury mainly as a result of the inability of injured axons to regenerate. Failure of mammalian CNS axon regeneration primarily occurs because of the presence of extrinsic inhibitory molecules and the lack of an intrinsic regenerative capacity of mature CNS neurons (Saijilafu et al., 2013a; Tateshita et al., 2018). Although several recent studies have drastically promoted mammalian CNS axon regeneration by experimentally increasing intrinsic axon growth ability (Liu et al., 2011; Filipp et al., 2019; Rodemer and Selzer, 2019), our understanding of cellular and molecular mechanisms by which axon regeneration is regulated remains rudimentary. Neurons in the mammalian peripheral nervous system retain the ability to regenerate through an axotomy-induced robust intrinsic growth response (Gey et al., 2016; Niemi, 2017; Duan et al., 2018), therefore providing a perfect model to dissect the underlying mechanisms of axon regeneration.

Sciatic nerve crush in rodents has been widely used as a model system to study peripheral axon regeneration *in vivo*. In this model, axon regeneration is often quantified using longitudinal nerve sections immunostained with specific axon regeneration-associated proteins, such as GAP43 and SCG10 (Abe et al., 2010; Shin et al., 2014). Because axon regeneration within nerve sections can only be quantified by measuring the fluorescent intensity of axon fragments at different distances from the crush site, this method provides only an indirect measurement of the lengths of regenerating axons. In addition, most nerve crush experiments are performed in places where both sensory axons from dorsal root ganglion (DRG) neurons and motor axons from the spinal cord motor neurons are mixed (Saijilafu et al., 2011; Liu et al., 2013; Ma et al., 2019). Therefore, the results represent average axon regeneration of two different neuronal populations that may have distinct axon regeneration abilities. Thus, the extent to which indirect measurements faithfully reflect real peripheral axon regeneration rate remains an open question. Electroporation, a rapid and effective method for gene delivery *in vivo*, has recently emerged as a powerful tool for studying in peripheral nerve regeneration. Our recently developed method for *in vivo* electroporation of plasmid DNA encoding for enhanced green fluorescent protein (EGFP) into adult sensory neurons in DRG provides a way to directly and specifically measure regenerating sensory axon lengths in whole-mount nerves. Here, we used this approach to quantify regenerating axon lengths after sciatic nerve crush at different time intervals.

Materials and Methods

Animals

Specific-pathogen-free 8- to 10-week-old male CF-1 mice weighing from 30 to 35 g were purchased from Charles River Laboratories (Wilmington, MA, USA) and housed in the University Animal Facility. There were six mice in each group. All mice were housed and treated according to protocols approved by the Institutional Animal Care and Use Committee of Guilin Medical University, China (approval No. GLMC201503010) on March 7, 2014.

Fluorescence labeling and sciatic nerve crush modeling

The rats were randomly divided into control and electroporation groups, which underwent a sham operation or a sciatic nerve crush + electroporation. Mice were anesthetized by intraperitoneal injection of a mixture of ketamine (100 mg/kg) and xylazine (10 mg/kg). *In vivo* electroporation of adult DRG neurons was performed as previously described (Saijilafu et al., 2011). Briefly, lumbar 4 (L4) and 5 (L5) DRGs on one side of the mouse were surgically exposed after anesthetization. A solution of DNA plasmid (pCMV-EGFP-N1, Clontech, Franklin Lakes, NJ, USA) encoding EGFP (1.0 μL) or a Dy547-tagged microRNA Hairpin Inhibitor (1.0 μL; GE Dharmacon, Chantilly, VA, USA) was injected into DRGs using a capillary pipette connected to a Picospritzer II (Parker Ins., Cleveland, OH, USA; 206.85-kPa pressure; 8-ms duration). Electroporation was then performed using a custom-made tweezer-like electrode and BTX ECM830 Electro Square Porator (five 15-ms pulses at 35 V with 950-ms interval). After DRG injection or electro-poration, the wound was closed and mice were allowed to recover from anesthesia. At 2 or 3 days after *in vivo* electroporation, the sciatic nerve on the side with electroporated DRGs was exposed and crushed at the sciatic notch (three 10-s crushes with forceps); the crush site was marked with 10-0 nylon epineural sutures. The wound was subsequently closed with 4-0 nylon sutures (Saijilafu et al., 2011).

Tissue preparation

For the axon regeneration rate study, at 12 and 18 hours, and 1, 2, 3, 4, 5, and 6 days after sciatic nerve crush, six mice were given a lethal overdose of ketamine/xylazine and then perfused transcardially with 20 mL of phosphate-buffered saline (pH 7.4), followed by 40 mL of ice-cold 4% paraformaldehyde at 5 mL/min. After perfusion, tissues were dissected out and post-fixed in 4% paraformaldehyde overnight at 4°C.

DRGs were first dehydrated in increasing concentrations of ethanol (50%, 70%, 80%, 90% and 100% for 30 minutes each) in amber glass bottles as previously described (Dodt et al., 2007; Luo et al., 2014; Belin et al., 2015). Incubations were carried out on an orbital shaker at room temperature. DRGs were then transferred into benzyl alcohol/benzyl benzoate (1:2 in volume; Sigma, St. Louis, MO, USA) clearing solution. During the procedure, tissues were protected from light to reduce the loss of fluorescent signal intensity.

Fluorescence imaging analysis of axon regeneration

Whole-mount cleared DRGs or sciatic nerves were imaged with a Zeiss LSM510 confocal microscope (Carl Zeiss MicroImaging, Oberkochen, Germany) controlled by LSM510 software. A 10× or 20× objective was used to acquire image stacks with 4–5-μm z spacing. The motor-driven XY scan-

ning stage with Mark & Find and Mosaic Scan function were used to scan DRG tissues with 15% overlap between X and Y dimensions. All acquired images were then merged together using LSM510 software to construct three-dimensional (3D) images or maximum intensity Z-projection images. Processing of fluorescence images and measurement of sensory axon regeneration were performed according to our previous studies (Hur et al., 2011; Zhang et al., 2014). Fluorescence images of fixed whole-mount nerve tissues were captured with an inverted fluorescence microscope controlled by the MosaicX module of AxioVision software (Carl Zeiss MicroImaging). All identifiable EGFP-labeled axons in whole-mount sciatic nerves were manually traced from the crush site to the distal axonal tips. At least 15 axons per nerve were measured and data from at least six mice for each experimental group were used to calculate mean axon lengths.

Western blot assay

DRG tissues were collected and lysed in RIPA buffer. Extracted proteins were separated sodium dodecyl sulfate-polyacrylamide gel (4–12% gradient) electrophoresis, and transferred onto polyvinylidene fluoride membranes. After blocking with 10% non-fat milk, membranes were incubated with primary antibodies (mouse anti-caspase-3; Cell Signaling Technology, Beverly, MA, USA; 1:100, 4°C, overnight) followed by a horseradish peroxidase-linked goat anti-mouse secondary antibody (Cell Signaling Technology, 1:3000) at room temperature for 1 hour. The densities of protein bands from three independent experiments were quantified using ImageJ software (NIH, Bethesda, MD, USA). The artificial unit of each protein was calculated by normalizing the band for the protein of interest to the band of the loading control, β-actin (mouse).

Statistical analysis

Regenerating sensory axon lengths were analyzed by one-way analysis of variance followed by *post-hoc* test with Dunnett's method. Statistical analysis was performed using GraphPad Prism 5.0 software (GraphPad Software, San Diego, CA, USA). A value of *P* < 0.05 was considered statistically significant.

Results

Time course analysis of sensory axon regeneration *in vivo*

Most previous studies of peripheral nerve regeneration quantified axon regeneration via indirect approaches. In addition, the results often represent average regeneration outcome of both sensory and motor axons. To directly measure the rate of sensory axon regeneration *in vivo*, we performed *in vivo* DRG electroporation combined with sciatic nerve crush as described in our previous studies (Hur et al., 2011; Saijilafu et al., 2011, 2013b; Liu et al., 2013; Zhang et al., 2014; Jiang et al., 2015). In brief, EGFP plasmid was transfected into L4 and L5 DRGs, followed by sciatic nerve crush at 2 days after electroporation. At different time points after crush, sciatic nerves were used for quantitative analysis of axon regeneration rate. The results showed that sensory axons regenerated

across the crush site and elongated gradually with time (**Figure 1A–H**). Average regenerating axon lengths at different time points are presented in **Figure 1I**. Sensory axons regenerated very slowly during the first day, but started to grow faster and steadily 2 days later. These results are consistent with previous *in vitro* studies indicating that adult mouse sensory neurons could switch into a regenerating mode after *in vitro* dissociation (axotomy) and 2 days in culture (Smith and Skene, 1997; Saijilafu et al., 2013b). Such time course data of *in vivo* mouse sensory axon regeneration provide an important reference for the axon regeneration field. We also imaged distal regenerating axons with regular confocal microscopy. The resulting 2D projection and 3D images showed clear depictions of regenerating growth cones (**Figure 2**).

Fluorescence-labeled DRGs and sensory axons

As shown above, whole-mount sciatic nerves with EGFP-labeled sensory axons could be imaged directly at high resolution without tissue clearing. However, the neuronal soma in DRGs could not be directly imaged because of their thickness. We previously showed EGFP-labeled neuronal soma using sectioned DRG tissues (Saijilafu et al., 2011). Thus, we examined if tissue clearing would help us obtain better images of whole-mount DRGs. Many approaches have been developed to clear mouse brains for 3D imaging (Richardson and Lichtman, 2015). Similar approaches have been used for mouse optic nerve clearing (Luo et al., 2014), and one recent study cleared sciatic nerves (Hu et al., 2016) for imaging axon regeneration and degeneration. One of these tissue-clearing approaches (Dodt et al., 2007; Belin et al., 2015) was used to clear DRGs and sciatic nerves. *In vivo* electroporation of EGFP plasmid DNA into L4 DRG was performed as previously described (Saijilafu et al., 2011). Three days after electroporation, the L4 DRG was dissected out with fragments of peripheral nerve and dorsal root attached. After tissue clearing, the DRG was imaged with a confocal microscope and a 3D image was constructed. Both the maximum projection image (**Figure 3A**) and 3D image (**Figure 3B**) clearly showed EGFP-labeled cell bodies of sensory neurons. In addition to expression of a gene of interest, we can also electroporate small RNA oligos (siRNAs) to knockdown protein translation (Saijilafu et al., 2013b) or regulate microRNA expression (microRNA mimics/inhibitors) (Liu et al., 2013; Jiang et al., 2015). However, in our previous studies, we only used western blot assay or reverse transcription-polymerase chain reaction to measure the functional results of siRNAs or microRNAs, respectively. To directly image small RNA oligos in sensory neurons, we electroporated a control mi-croRNA inhibitor tagged with the fluorescent dye Dy547 into DRGs. Most cell bodies in DRGs were strongly labeled with Dy547 at 1 day after electroporation (**Figure 3C, D**). Because of the tissue clearing technique used here, processed whole-mount tissues were not optimally compatible for immunostaining. Thus, we did not perform neuronal marker labeling to quantify the transfection efficiency. Nevertheless, images of cleared DRG tissues obviously showed that the transfection efficiency of small RNA oligos was much higher than that of EGFP, be-
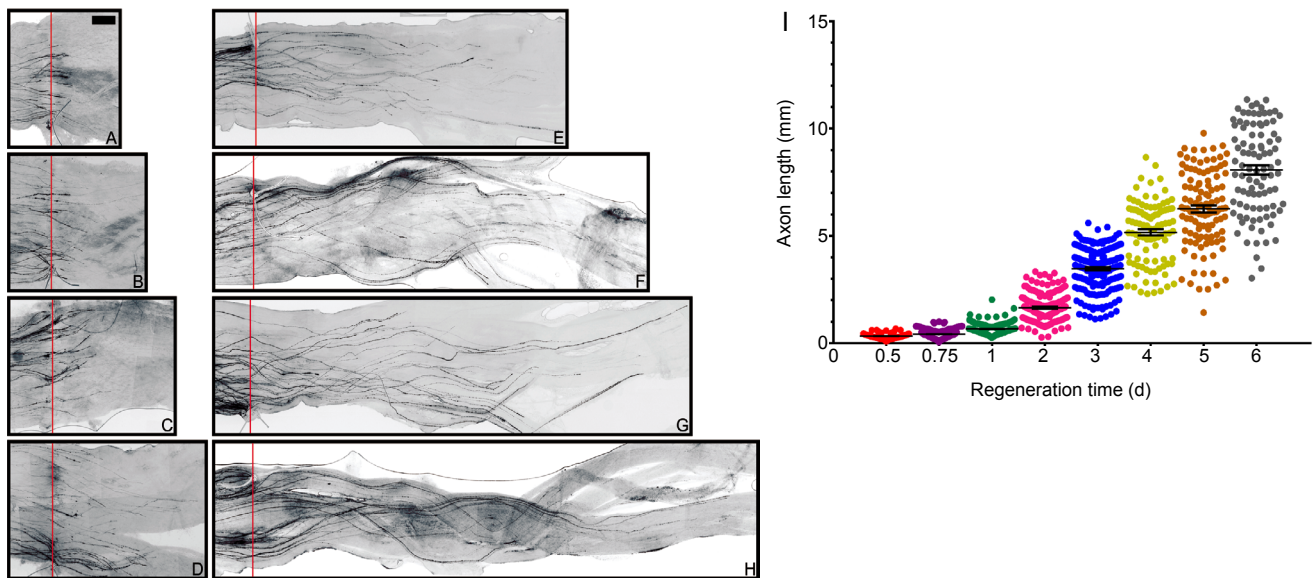
Figure 1 Representative images and quantification of regenerating sensory axons at different time points after nerve crush.
(A–H) At 12 and 18 hours, and 1, 2, 3, 4, 5, and 6 days, the length of each regenerating axon was measured from the crush site to the distal axonal tip. Red lines indicate crush sites. Scale bar: 500 μm. (I) Average lengths of regenerating sensory axons at different time points after nerve crush (*n* = 6 mice per group at 12 and 18 hours, and 1, 2, 3, 4, 5, and 6 days after nerve crush).
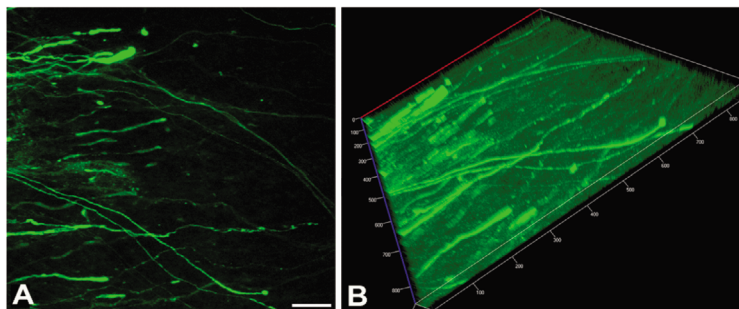
Figure 2 Representative confocal images of distal regenerating sensory axons labeled with enhanced green fluorescent protein at 2 days after surgery.
(A) Maximum projection image; (B) reconstructed three-dimensional image. Scare bar: 100 μm.
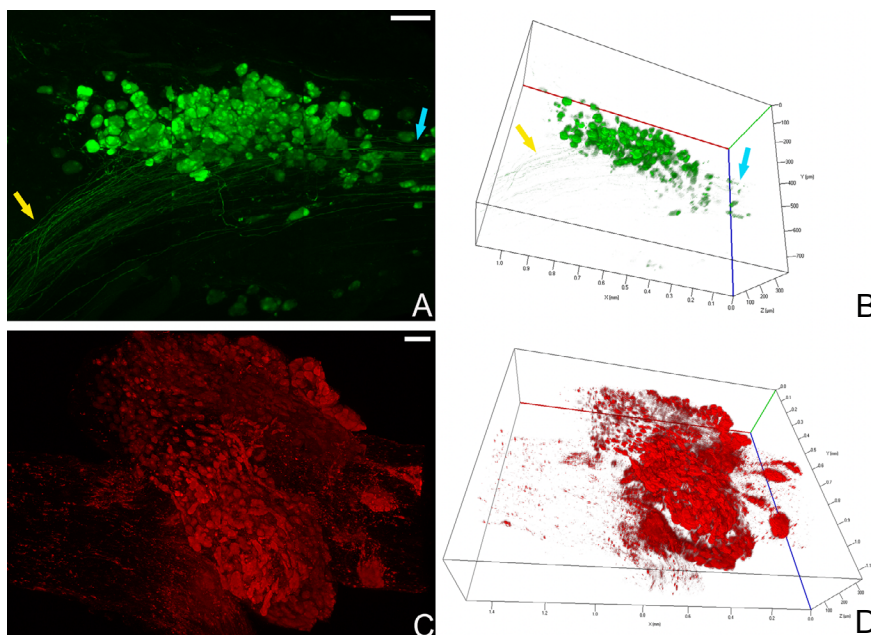
Figure 3 Tissue clearing and 3D imaging of whole-mount DRG electroporated with EGFP plasmid and fluorescent dye-tagged microRNA inhibitor.
(A) Maximum projection image of EGFP-positive sensory neuron cell bodies 3 days after electroporation: attached EGFP-labeled peripheral axon branches (yellow arrow) and central axon branches (blue arrow) were also visible. Scale bar: 100 μm. (B) Reconstructed 3D image of electroporated DRG expressing EGFP. (C) Maximum projection image of DRG labeled with Dy547-tagged microRNA inhibitor. Scale bar: 100 μm. (D) Reconstructed 3D image of electroporated DRG expressing microRNA inhibitor. 3D: Three-dimensional; DRG: dorsal root ganglion; EGFP: enhanced green fluorescent protein.

cause the electroporation efficiency was mainly determined by the size of transfected materials. For sciatic nerves, the tissue clearing approach resulted in a good clearing effect (**Figure 4**).

Electroporation does not affect cell apoptosis in DRGs

Our previous result revealed no observable signs of tissue damage or cell abnormalities, indicating that neither injection nor electroporation caused obvious cell death (Saijilafu et al., 2011). Moreover, using electroporation methods to transfect microRNA and EGFP to DRGs did not induce caspase-3 activation, a widely used marker of apoptosis (Hu et al., 2016). Here, we also collected DRGs, which were transfected EGFP by electroporation 3 days and 7 days later. Western blot assay results for caspase-3 protein indicated no significant difference between control and electroporation groups ($P > 0.05$; **Figure 5**).

Discussion

Peripheral nerve regeneration is an important model system to study the cellular and molecular mechanisms by which mammalian axon regeneration is regulated. Our previous studies showed that *in vivo* electroporation of DRGs combined with sciatic nerve crush injury provides a powerful tool to study axon regeneration *in vivo* (Hur et al., 2011; Liu et al., 2013; Saijilafu et al., 2013b; Zhang et al., 2014). Importantly, *in vivo* electroporation has many advantages over conventional transgenic or viral-mediated genetic approaches, such as shorter experimental time, more precise temporal control of gene expression, and direct measurement of axon lengths *in vivo*. Here, using such a model, we first analyzed the lengths of regenerating sensory axons *in vivo* at different time points after nerve crush. The results provided reliable time-dependent *in vivo* sensory axon regeneration rates, which can serve as an important reference for future studies of peripheral axon regeneration. In addition, by specifically labeling motor axons with fluorescence dye, in the future we can investigate if motor and sensory neurons have different axon regeneration rates *in vivo* within a similar peripheral nerve environment. In this study, a tissue-clearing approach was next used to successfully clear DRGs and sciatic nerves. Three-dimensional imaging of cleared DRGs provided higher quality images of sensory neurons expressing EGFP or fluorescent dye-tagged small RNA oligos. A recent study comprehensively investigated peripheral axon regeneration using tissue clearing and whole-mount tissue immunostaining (Jung et al., 2014; Jiang et al., 2015). Our study only used a quick tissue clearing approach to image sensory axons and DRGs pre-labeled with a fluorescent protein or dye. In the future, by directly tracing the central branches of sensory
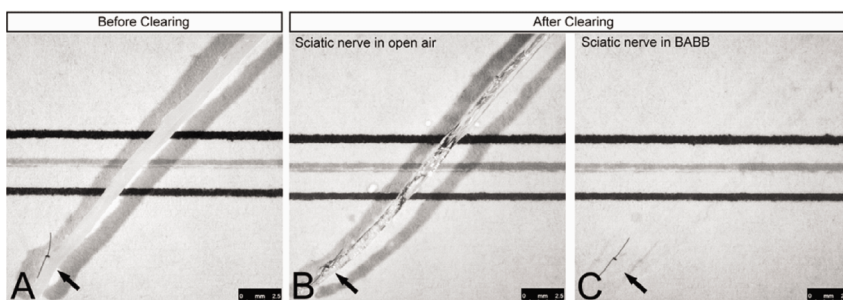

Figure 4 Representative sciatic nerve samples before and after tissue clearing.
(A) Sciatic nerve before tissue clearing. (B) The same sciatic nerve after clearing in open air. (C) Sciatic nerve after clearing in benzyl alcohol/benzyl benzoate. Black arrows indicate the crush site labeled with the suture.
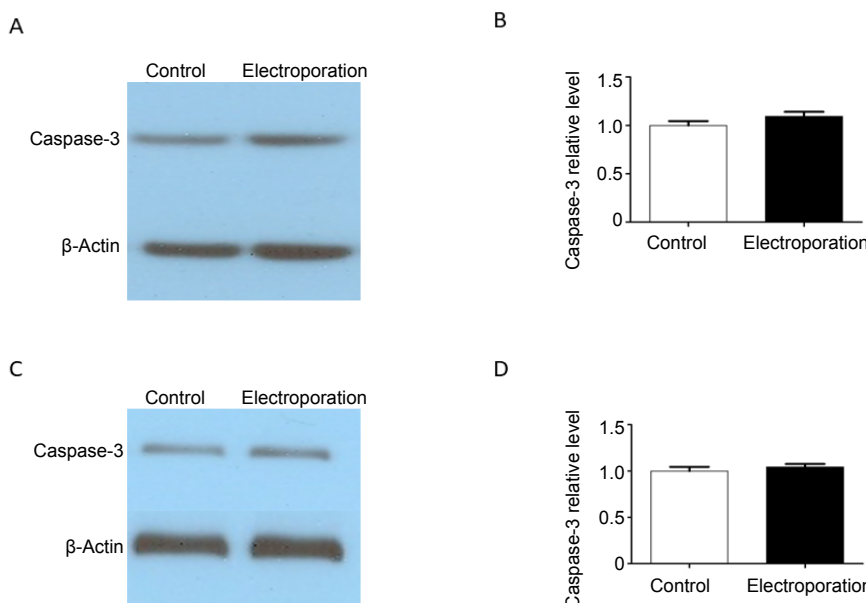

Figure 5 Western blot assay results of DRG in the control and electroporation groups.
(A) Representative western blot images of caspase-3 in adult mouse DRG 3 days after electroporation. (B) Quantification of caspase-3 levels (normalized to actin, $n = 3$ for each condition). (C) Representative western blot images of caspase-3 in adult mouse DRG by electroporation 7 days later. (D) Quantification of caspase-3 levels (normalized to actin, $n = 3$ for each condition). Data are expressed as the mean ± SEM (one-way analysis of variance followed by *post-hoc* test with Dunnett's method). DRG: Dorsal root ganglion.

neurons combined with tissue clearing of the spinal cord, our approach can be used to investigate spinal cord regeneration at high throughput and with good resolution.

Institutional review board statement: *The study was approved by the Institutional Animal Care and Use Committee of Guilin Medical University, China (approval No. GLMC201503010) on March 7, 2014.*

Data sharing statement: *Datasets analyzed during the current study are available from the corresponding author on reasonable request.*

Plagiarism check: *Checked twice by iThenticate.*

Peer review: *Externally peer reviewed.*

Open peer reviewer: *André Poot, University of Twente, Netherlands.*

References

Abe N, Borson SH, Gambello MJ, Wang F, Cavalli V (2010) Mammalian target of rapamycin (mTOR) activation increases axonal growth capacity of injured peripheral nerves. J Biol Chem 285:28034-28043.

Belin S, Nawabi H, Wang C, Tang S, Latremoliere A, Warren P, Schorle H, Uncu C, Woolf CJ, He Z, Steen JA (2015) Injury-induced decline of intrinsic regenerative ability revealed by quantitative proteomics. Neuron 86:1000-1014.

Dodt HU, Leischner U, Schierloh A, Jahrling N, Mauch CP, Deininger K, Deussing JM, Eder M, Zieglgansberger W, Becker K (2007) Ultramicroscopy: three-dimensional visualization of neuronal networks in the whole mouse brain. Nat Methods 4:331-336.

Duan RS, Tang GB, Du HZ, Hu YW, Liu PP, Xu YJ, Zeng YQ, Zhang SF, Wang RY, Teng ZQ, Liu CM (2018) Polycomb protein family member CBX7 regulates intrinsic axon growth and regeneration. Cell Death Differ 25:1598-1611.

Filipp ME, Travis BJ, Henry SS, Idzikowski EC, Magnuson SA, Loh MY, Hellenbrand DJ, Hanna AS (2019) Differences in neuroplasticity after spinal cord injury in varying animal models and humans. Neural Regen Res 14:7-19.

Gey M, Wanner R, Schilling C, Pedro MT, Sinske D, Knoll B (2016) Atf3 mutant mice show reduced axon regeneration and impaired regeneration-associated gene induction after peripheral nerve injury. Open Biol 6:160091.

Hu YW, Jiang JJ, Yan G, Wang RY, Tu GJ (2016) MicroRNA-210 promotes sensory axon regeneration of adult mice in vivo and in vitro. Neurosci Lett 622:61-66.

Hur EM, Saijilafu, Lee BD, Kim SJ, Xu WL, Zhou FQ (2011) GSK3 controls axon growth via CLASP-mediated regulation of growth cone microtubules. Genes Dev 25:1968-1981.

Jiang JJ, Liu CM, Zhang BY, Wang XW, Zhang M, Saijilafu, Zhang SR, Hall P, Hu YW, Zhou FQ (2015) MicroRNA-26a supports mammalian axon regeneration in vivo by suppressing GSK3β expression. Cell Death Dis 6:e1865.

Jung Y, Ng JH, Keating CP, Senthil-Kumar P, Zhao J, Randolph MA, Winograd JM, Evans CL (2014) Comprehensive evaluation of peripheral nerve regeneration in the acute healing phase using tissue clearing and optical microscopy in a rodent model. PLoS One 9:e94054.

Liu CM, Wang RY, Saijilafu, Jiao ZX, Zhang BY, Zhou FQ (2013) MicroRNA-138 and SIRT1 form a mutual negative feedback loop to regulate mammalian axon regeneration. Genes Dev 27:1473-1483.

Liu K, Tedeschi A, Park KK, He Z (2011) Neuronal intrinsic mechanisms of axon regeneration. Annu Rev Neurosci 34:131-152.

Luo X, Yungher B, Park KK (2014) Application of tissue clearing and light sheet fluorescence microscopy to assess optic nerve regeneration in unsectioned tissues. Methods Mol Biol 1162:209-217.

Ma JJ, Xu RJ, Qi SB, Wang F, Ma YX, Zhang HC, Xu JH, Qin XZ, Zhang HN, Liu CM, Li B, Chen JQ, Yang HL, Saijilafu (2019) Regulation of adult mammalian intrinsic axonal regeneration by NF-kappaB/STAT3 signaling cascade. J Cell Physiol doi: 10.1002/jcp.28815.

Niemi JP (2017) Macrophage accumulation near injured neuronal cell bodies is necessary and sufficient for peripheral axon regeneration. Cleveland, USA: Case Western Reserve University School of Graduate Studies.

Richardson DS, Lichtman JW (2015) Clarifying tissue clearing. Cell 162:246-257.

Rodemer W, Selzer ME (2019) Role of axon resealing in retrograde neuronal death and regeneration after spinal cord injury. Neural Regen Res 14:399-404.

Saijilafu, Hur EM, Zhou FQ (2011) Genetic dissection of axon regeneration via in vivo electroporation of adult mouse sensory neurons. Nat Commun 2:543.

Saijilafu, Zhang BY, Zhou FQ (2013a) Signaling pathways that regulate axon regeneration. Neurosci Bull 29:411-420.

Saijilafu, Hur EM, Liu CM, Jiao Z, Xu WL, Zhou FQ (2013b) PI3K-GSK3 signalling regulates mammalian axon regeneration by inducing the expression of Smad1. Nat Commun 4:2690.

Shin JE, Geisler S, DiAntonio A (2014) Dynamic regulation of SCG10 in regenerating axons after injury. Exp Neurol 252:1-11.

Smith DS, Skene JH (1997) A transcription-dependent switch controls competence of adult neurons for distinct modes of axon growth. J Neurosci 17:646-658.

Tateshita T, Ueda K, Kajikawa A (2018) End-to-end and end-to-side neurorrhaphy between thick donor nerves and thin recipient nerves: an axon regeneration study in a rat model. Neural Regen Res 13:699-703.

Zhang BY, Saijilafu, Liu CM, Wang RY, Zhu Q, Jiao Z, Zhou FQ (2014) Akt-independent GSK3 inactivation downstream of PI3K signaling regulates mammalian axon regeneration. Biochem Biophys Res Commun 443:743-748.